Research Article (Supplementary Material)

Domenico Genchi*, Francesca Dodici, Tiziana Cesca, and Giovanni Mattei

Design of optical Kerr effect in multilayer hyperbolic metamaterials

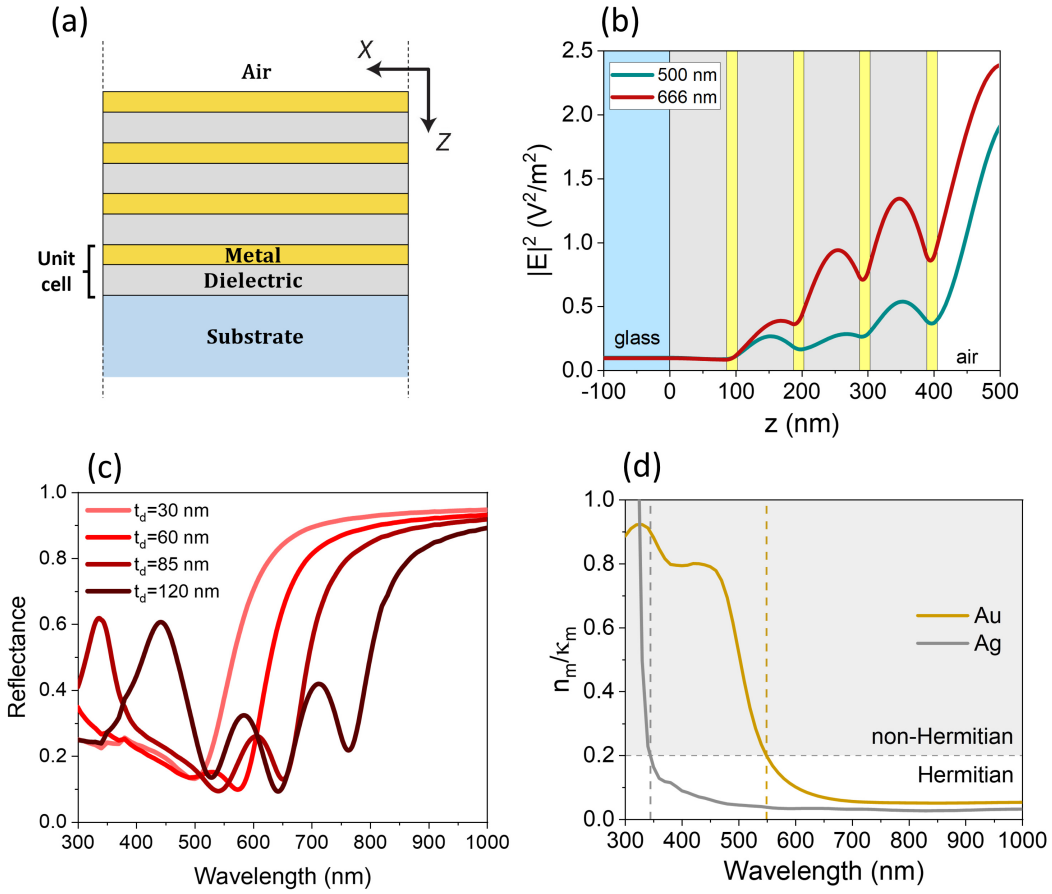

Fig. S1: (a) Sketch of the multilayer metamaterials. (b) Profile of the electric field ($|E|^2$) within a four-period 15/85 Au/Al_2O_3 metamaterial, simulated by EMUstack at λ=500 nm (green curve) and λ_{ENZ}=666 nm (red curve); the incident wave has an amplitude of 1 V/m and comes from the air side, where both the input and reflected contributions are present. (c) Reflectance of Au/Al_2O_3 HMs with different metal filling fraction, varied by changing the thickness of the dielectric layers while maintaining that of the metal layers equal to 15 nm. (d) Ratio between refractive index and extinction coefficient of Au and Ag, defining the "hermiticity limit" for the sustain of ENZ resonances. Below the critical value (Hermitian system) the wave energy is conserved, i.e. the wave does not lose or gain energy while propagating, and ENZ resonances can exist; conversely, above the critical value (non-Hermitian system), the wave can be amplified or damped through a non-conservative exchange of energy with the surrounding medium, so the cavity resonances are strongly quenched (e.g. in the spectral region of the metal interband transitions, where the ratio n_m/κ_m is very large) [1, 2].

***Corresponding author: Domenico Genchi,** University of Padua, NanoStructures Group (NSG), Dept. of Physics and Astronomy (DFA), Via Marzolo 8, 35131 Padua (Italy), e-mail: domenico.genchi@unipd.it
Francesca Dodici, Tiziana Cesca, Giovanni Mattei, University of Padua, NanoStructures Group (NSG), Dept. of Physics and Astronomy (DFA), Via Marzolo 8, 35131 Padua (Italy)

Sample	t_m (nm)	t_d (nm)	t_{tot} (nm)	R_{RMS} (nm)
Au/Al_2O_3 15/30	14.9±0.9	30±2	185±10	1.2±0.1
Au/Al_2O_3 15/60	16.6±0.2	65.8±0.8	320±5	1.0±0.2
Au/Al_2O_3 15/85 (AuAlu16)	15.6±1.2	85±5	420±20	0.9±0.1
Au/Al_2O_3 15/120	16.6±0.3	121±2	550±30	0.5±0.1
Au/Al_2O_3 10/52	10.5±0.9	54±5	255±13	0.7±0.2
Au/Al_2O_3 20/105	20±2	100±10	490±20	0.9±0.2
Au/Al_2O_3 10/20	9±2	19±1	121±6	1.4±0.4
Au/Al_2O_3 20/40	18.7±0.9	38±2	233±12	1.5±0.3
Ag/Al_2O_3 15/85 (AgAlu16)	16±3	90±20	409±20	2.5±0.6

Tab. S1: Morphological parameters of the fabricated metamaterials. The thickness of the metal layers (t_m) and dielectric layers (t_d) are determined by ellipsometry, whereas the total thickness (t_{tot}) and the average roughness (R_{RMS}) are measured by AFM.

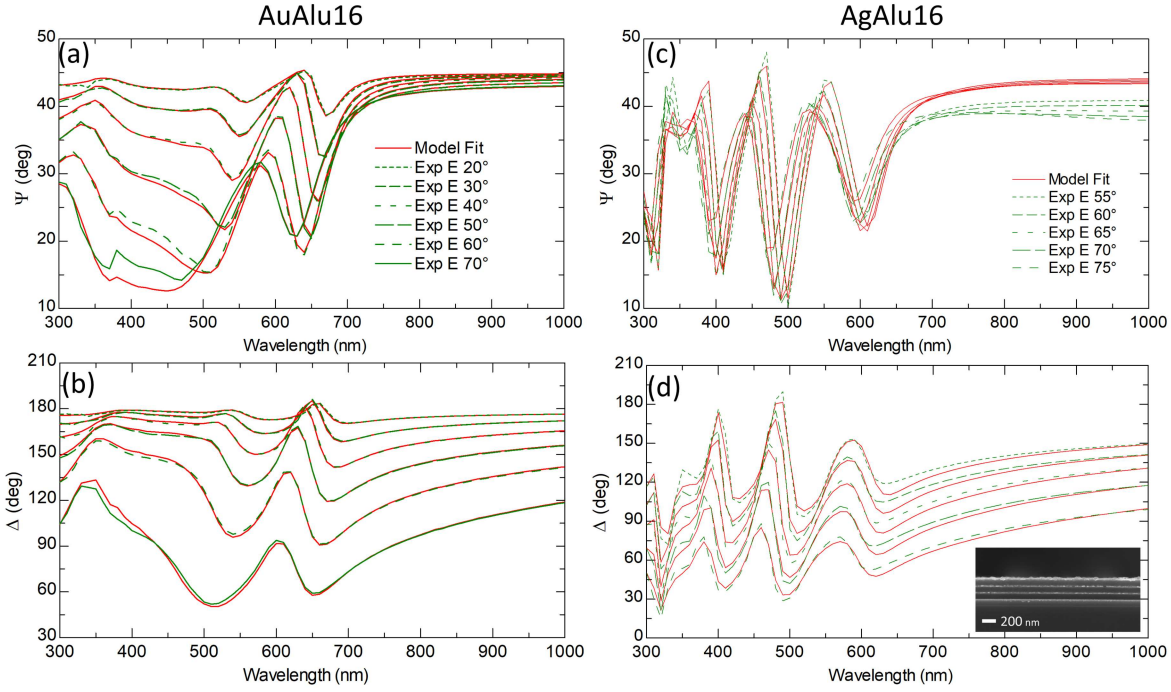

Fig. S2: Angle-resolved spectroscopic ellipsometry measurements performed on the samples AuAlu16 (a,b) and AgAlu16 (c,d). The experimental data (green) of the ellipsometric parameters Ψ (amplitude ratio, (a,c)) and Δ (phase shift, (b,d)), conventionally expressed as angles, are fitted by the simulated curves (red). The fit is obtained implementing the experimental permittivities of the constituent materials previously obtained by ellipsometric measurements performed on reference samples (Au 15 nm and 60 nm; Al_2O_3 85 nm, Ag 15 nm). These are reported in Fig. S3, and they are fixed in the multilayer model for the ellipsometric analysis, so that the thickness of the layers is the only free parameter. The model implemented for the simulation of the optical transmittance and the ellipsometric fit includes 3 nm intermix between the silver and alumina layers of the metamaterial, and slight oxidation (2%) of the silver layers, to account for possible clustering and oxidation effects at the Ag interfaces due to a low silver-alumina interaction (namely low interfacial surface tension) and Ag-O bonding at the first adsorption steps during the layers depositions [3, 4]. The inset in panel (d) depicts a cross-sectional SEM image of AgAlu16.

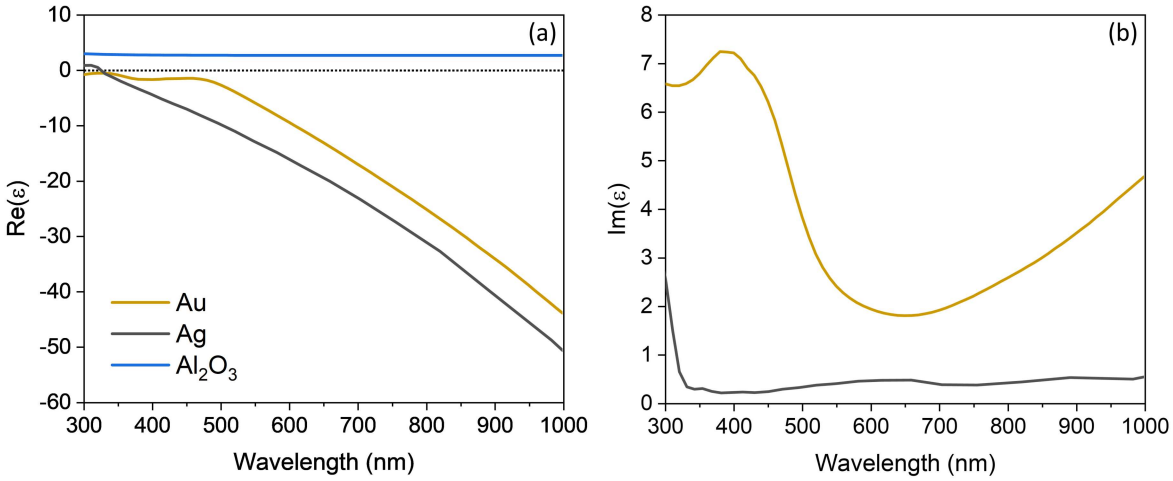

Fig. S3: (a) Real part and (b) imaginary part of the permittivity of the materials constituting the metamaterials of this work.

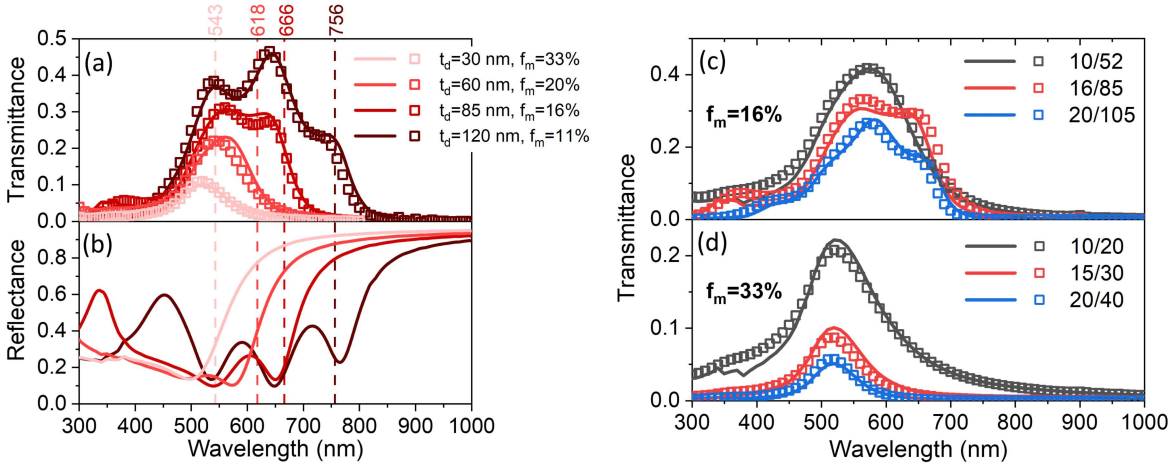

Fig. S4: (a) Transmittance and (b) reflectance spectra of fabricated HMs with t_m=15 nm and different t_d, i.e. variable f_m. (c,d) Transmittance of fabricated HMs with equivalent f_m and different layers thickness. The open symbols and the solid curves are the experimental and simulated spectra respectively. The vertical dashed lines indicate their ENZ wavelengths. In (a) the transmittance window can be broadened by increasing the thickness of the dielectric layers, that is lowering the metal filling fraction, so that a higher number of PP modes are sustained. The nature of these modes is confirmed by the transmittance peaks in (a) and the reflectance dips in (b), corresponding to the absorptance peaks in Fig. 1(b) of the main text. In (c,d) it is shown that the effect of PPs plays a more important role in metamaterials with low filling fraction, significantly modifying the spectral shape of their optical features. Indeed, with f_m=16% the transmittance window is strongly modulated by increasing the thickness of the layers, that is activating the effect of PPs that strongly alter the propagation of the transmitted wave. Differently, with f_m=33% the response of the metal dominates so that only the transmittance band due to the crossover between the interband and intraband transitions of gold appear, and this drops in absolute value with thicker layers, namely with higher metal absorption.

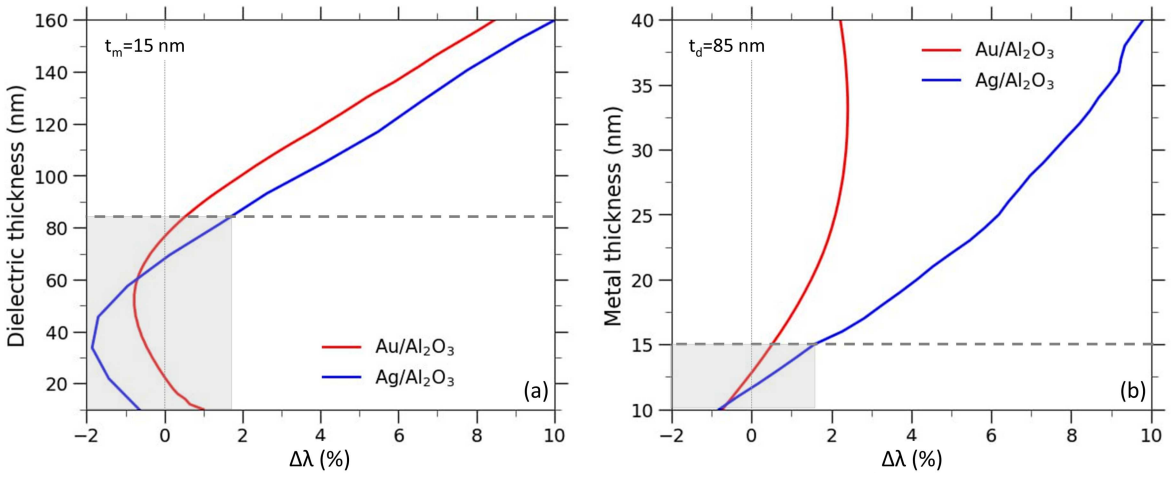

Fig. S5: Percent deviation between λ_{ENZ}^{ISMM} and λ_{ENZ}^{EMT}, calculated as $\Delta\lambda_{ENZ}(\%) = [\lambda_{ENZ}^{ISMM} - \lambda_{ENZ}^{EMT}]/\lambda_{ENZ}^{ISMM}$ for Au/Al_2O_3 (red) and Ag/Al_2O_3 (blue) four-period metamaterials with (a) 15 nm metal thickness as a function of the dielectric thickness, and (b) 85 nm dielectric thickness as a function of the metal thickness. The horizontal dashed line indicates the layers thickness at which the values of λ_{ENZ}^{EMT} and λ_{ENZ}^{ISMM} start to significantly diverge (see also Fig. 2(a,d)), while the gray area indicates the thickness range within which they approximately coincide.

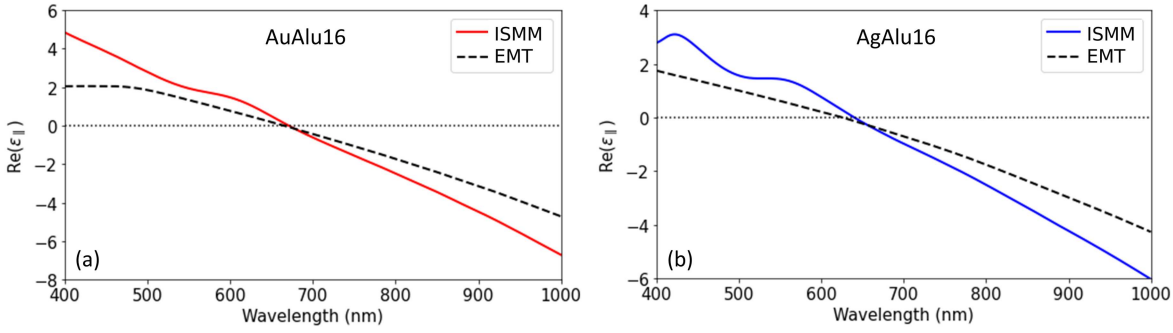

Fig. S6: Comparison between the effective permittivity (parallel, real part) calculated by effective medium theory (EMT, dashed curves) and inverse scattering matrix method (ISMM, solid lines) for AuAlu16 (a) and AgAlu16 (b).

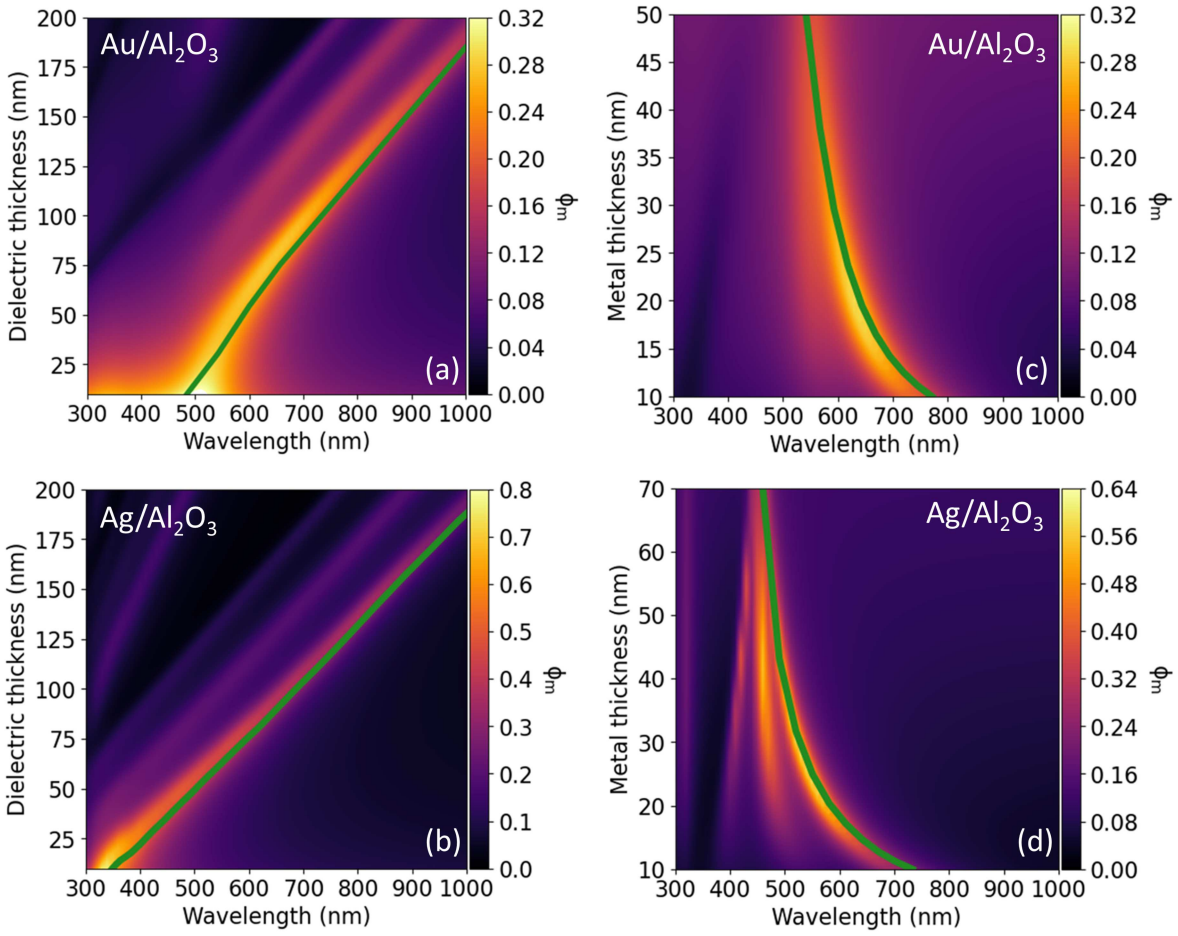

Fig. S7: Effective filling fraction ϕ_m spectrally calculated for (a,c) Au/Al_2O_3 and (b,d) Ag/Al_2O_3 hyperbolic metamaterials as a function of (a,b) the dielectric layers thickness (with 15 nm metal layers), and (c,d) the metal layers thickness (with 85 nm dielectric thickness). The green curves are the locus of points of the ENZ wavelengths calculated by ISMM for each geometrical combination.

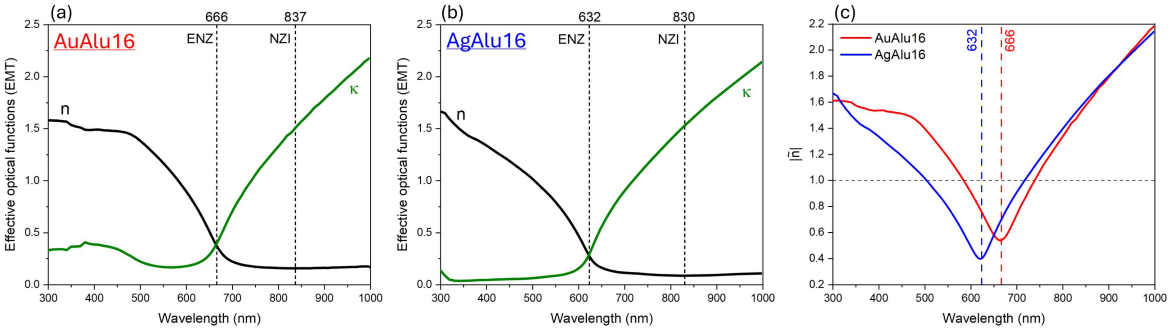

Fig. S8: (a,b) Effective optical functions (refractive index n and extinction coefficient κ) calculated by EMT as a function of wavelength for the samples AuAlu16 and AgAlu16. The vertical dashed lines indicate the ENZ and NZI wavelengths. (c) Modulus of the complex effective refractive index calculated as a function of wavelength from the optical functions in (a,b). The vertical dashed lines indicate the minimum value of $|\tilde{n}|$ coinciding with the ENZ wavelength. The horizontal dashed line delimits the bandwidth where $|\tilde{n}| < 1$ and NZI effects occur.

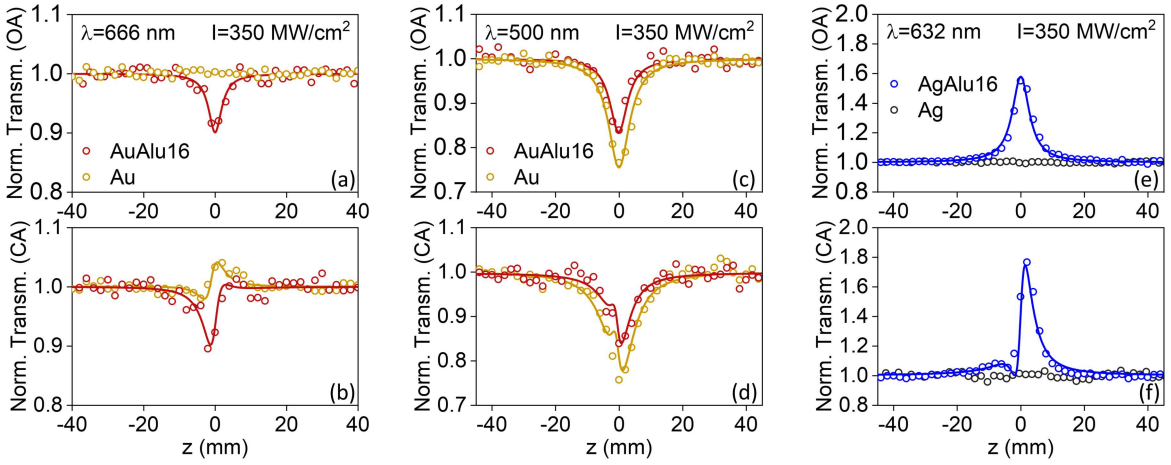

Fig. S9: Z-scan curves measured at normal incidence for (a-d) AuAlu16 (red) compared to Au thin film (gold), and for (e-f) AgAlu16 (blue) compared to Ag thin film (gray). The measurements in (a-b, e-f) are performed at the ENZ wavelengths of the metamaterials, whereas those in (c-d) are taken at λ=500 nm. The open circles are the experimental data, and the solid lines are the best-fitting curves. The following values of the nonlinear parameters are extracted from the presented measurements: (a-b) at 666 nm AuAlu16 has β=4×10^{-5} cm/W and n_2=3×10^{-10} cm^2/W, while Au has n_2=2×10^{-10} cm^2/W; (c-d) at 500 nm AuAlu16 has β=5.5×10^{-4} cm/W and n_2=-6×10^{-10} cm^2/W, while Au has β=5×10^{-3} cm/W) and n_2=4×10^{-9} cm^2/W; (e-f) at 632 nm AgAlu16 has β=-4×10^{-4} cm/W) and n_2=2×10^{-9} cm^2/W.

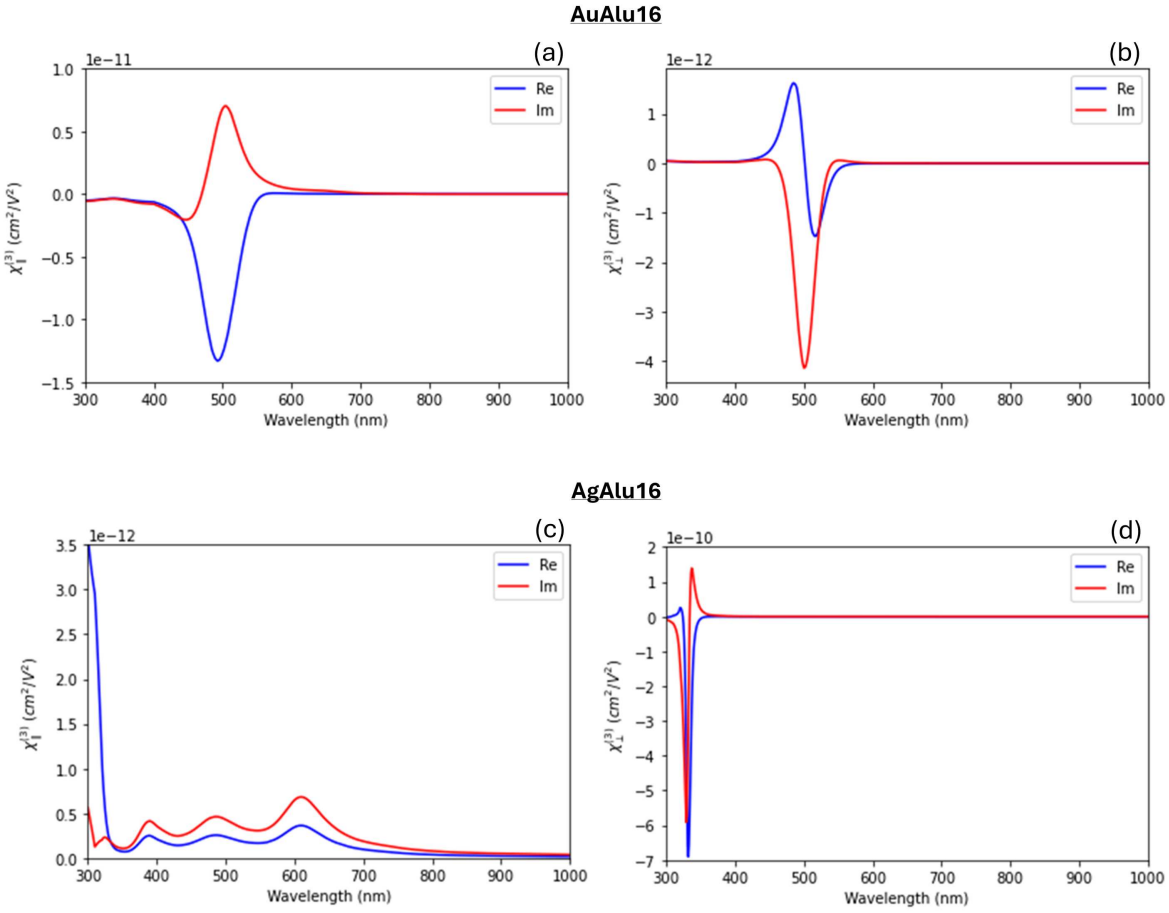

Fig. S10: Effective third-order susceptibility (parallel and perpendicular components) calculated for the samples AuAlu16 (a-b) and AgAlu16 (c-d).

Au/Al_2O_3 sample	n_2 $(10^{-10}\mathrm{cm}^2/\mathrm{W})$			β $(10^{-4}\mathrm{cm}/\mathrm{W})$		
	Norm. Inc.	TE 60°	TM 60°	Norm. Inc.	TE 60°	TM 60°
15/30	11 ± 2	5 ± 2	4 ± 1	3.7 ± 0.6	2.2 ± 0.8	1.2 ± 0.6
15/85	3.3 ± 0.9	0.9 ± 0.3	1.6 ± 0.8	0.40 ± 0.06	0.07 ± 0.04	0.07 ± 0.02
15/120	1.2 ± 0.4	–	–	0.07 ± 0.03	–	–
10/52	4.2 ± 0.4	1.6 ± 0.7	1.6 ± 0.3	0.22 ± 0.02	0.12 ± 0.03	0.04 ± 0.01
20/105	1.8 ± 0.3	0.7 ± 0.2	0.8 ± 0.2	0.23 ± 0.02	n.a.	0.10 ± 0.04
10/20	13 ± 2	10 ± 2	5 ± 1	4.6 ± 0.5	1.9 ± 0.9	0.80 ± 0.08
20/40	10 ± 2	4 ± 1	4.0 ± 0.6	6 ± 1.0	0.7 ± 0.2	1.5 ± 0.2

Tab. S2: Nonlinear refractive index (n_2) and nonlinear absorption coefficient (β) measured in different configurations (angle and polarization) at λ_{ENZ} for the fabricated Au/Al_2O_3 metamaterials.

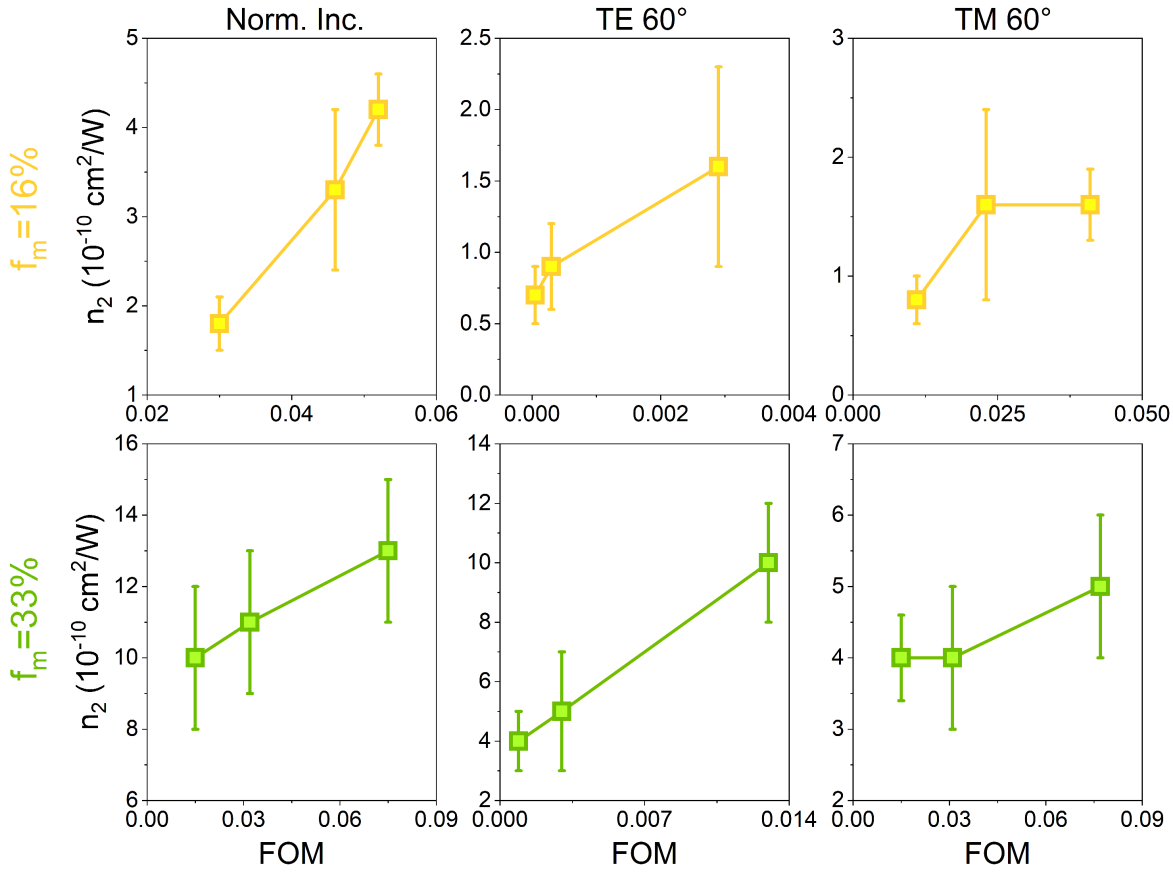

Fig. S11: Trend of nonlinear refractive index as a function of the FOM for multilayer HMs with f_m=16% and f_m=33% (considered in Fig. 5 of the main text) measured at their λ_{ENZ} (respectively 666 nm and 543 nm).

References

[1] V. Caligiuri, M. Palei, G. Biffi, S. Artyukhin, and R. Krahne, "A semi-classical view on epsilon-near-zero resonant tunneling modes in metal/insulator/metal nanocavities," *Nano Letters*, vol. 19, pp. 3151–3160, 2019.

[2] C. Coulais, R. Fleury, and J. van Wezel, "Topology and broken hermiticity," *Nature Physics*, vol. 17, pp. 9–13, 2021.

[3] K. Luo, X. Lai, C. W. Yi, K. A. Davis, K. K. Gath, and D. W. Goodman, "The growth of silver on an ordered alumina surface," *Journal of Physical Chemistry B*, vol. 109, pp. 4064–4068, 2005.

[4] D. Guo, Q. Guo, K. Zheng, E. G. Wang, and X. Bao, "Initial growth and oxygen adsorption of silver on Al_2O_3 film," *The Journal of Physical Chemistry C*, vol. 111, pp. 3981–3985, 3 2007.